# Observed and Calculated Downwelling Longwave Spectral Radiances at the SHEBA Ice Station: Prelude to an Arctic AERI/LBLRTM QME

*D. C. Tobin, R. O. Knuteson, and H. E. Revercomb*
*Cooperative Institute for Meteorological Satellite Studies*
*Space, Science, and Engineering Center*
*University of Wisconsin*
*Madison, Wisconsin*

## Introduction

We present comparisons of clear-sky observed and calculated downwelling radiances from the year-long Surface Heat Budget of the Arctic Ocean (SHEBA) experiment. These and expected similar comparisons from the Atmospheric Radiation Measurement (ARM) North Slope of Alaska (NSA) site in Barrow, Alaska, are useful for assessing the accuracy of clear-sky forward model issues, particularly the far-infrared air-broadened water vapor continuum and the temperature dependence of the 8 μm to 12 μm self-broadened water vapor continuum, as well for assessing the accuracy of measured atmospheric temperature and water vapor profiles. This work is an extension of the original atmospheric emitted radiance interferometer/line-by-line radiative transfer model (AERI/LBLRTM) Quality Measurement Experiment (QME), which has been ongoing at the Southern Great Plains (SGP) site since 1994, and of an analysis of several clear-sky SHEBA case studies consisting of AERI-equivalent radius (ER) measurements and collocated radiosondes, which led to recent changes in the CKD representation of the far-infrared air-broadened water vapor continuum.

This analysis draws upon a number of measurements collected during SHEBA including Vaisala RS-80 radiosonde profiles of temperature and water vapor, ARM microwave radiometer (CMWR) measurements of integrated column vapor and liquid water, AERI measurements of spectral downwelling radiance, and the Environmental Technology Laboratory (ETL) DABUL Lidar cloud measurements. The calculations were performed with LBLRTM with the CKDv2.4 water vapor continuum.

## Selection of Clear Skies

The ETL Lidar cloud height data product, microwave radiometer (MWR) liquid water, and AERI radiances were used to determine clear-sky periods. Requiring clear skies for 5 minutes before and 45 minutes after the 11:15 Universal Time Coordinates (UTC) and 23:15 UTC radiosonde launches, and requiring all necessary data (sondes, CMWR, Lidar, and AERI) limits the number of clear-sky cases to 62. These radiosonde profiles are shown in Figure 1. These occurred between December 1997 and May 1998, with integrated column water vapor values between 0.08 cm and 0.5 cm, and near surface air temperatures between -40°C and -10°C. Time series of relevant parameters are shown in Figure 2. For a limited number of cases, the AERI radiances exhibited small changes with time that did not correlate

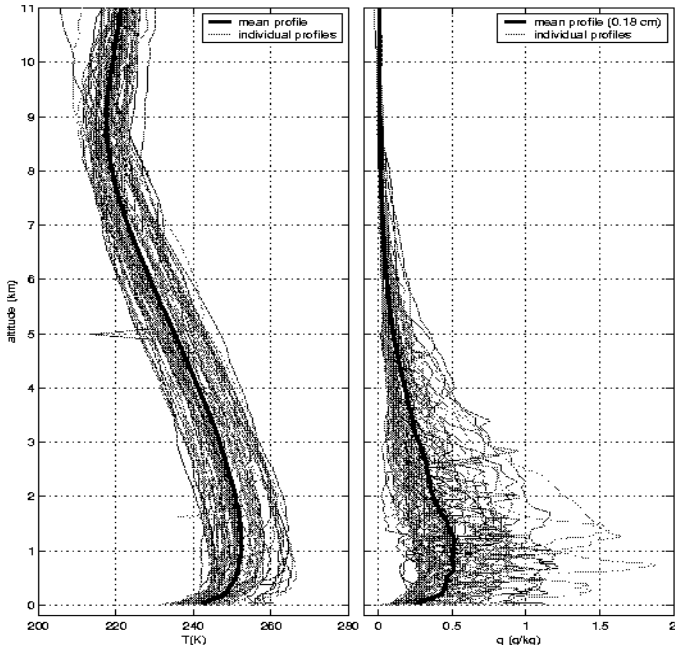


**Figure 1**. Clear-sky radiosonde profiles.

with water vapor when clouds were not detected. An example is given in Figure 3. We suspect this is due to very thin low clouds or to the ship's exhaust. To exclude these time periods, an additional constraint of requiring the 9 minus 12 μm AERI brightness temperature differences to be greater than 25K was used, as shown in Figure 4.

## Simulated Spectral Residuals

To simulate errors in the calculated radiances, calculations were performed using the mean radiosonde profile with various perturbations to the input profiles and model absorption coefficients. These include changes in the input water vapor profile and the self ($C_s^0$) and air ($C_f^0$) broadened water vapor continuum coefficients. These are given in Figures 5 and 6 along with the unperturbed downwelling calculation and surface-to-space transmission, all at AERI spectral resolution.

## Integrated Column Water Vapor Measurements

Figures 7 and 8 show comparisons of the radiosonde and CMWR integrated water vapor measurements. The CMWR values are 50-minute averages around the sonde launch times (5 minutes before and 45 minutes after launch). For the dry, clear-sky time periods, the radiosonde values are roughly 30% dryer than the CMWR values.

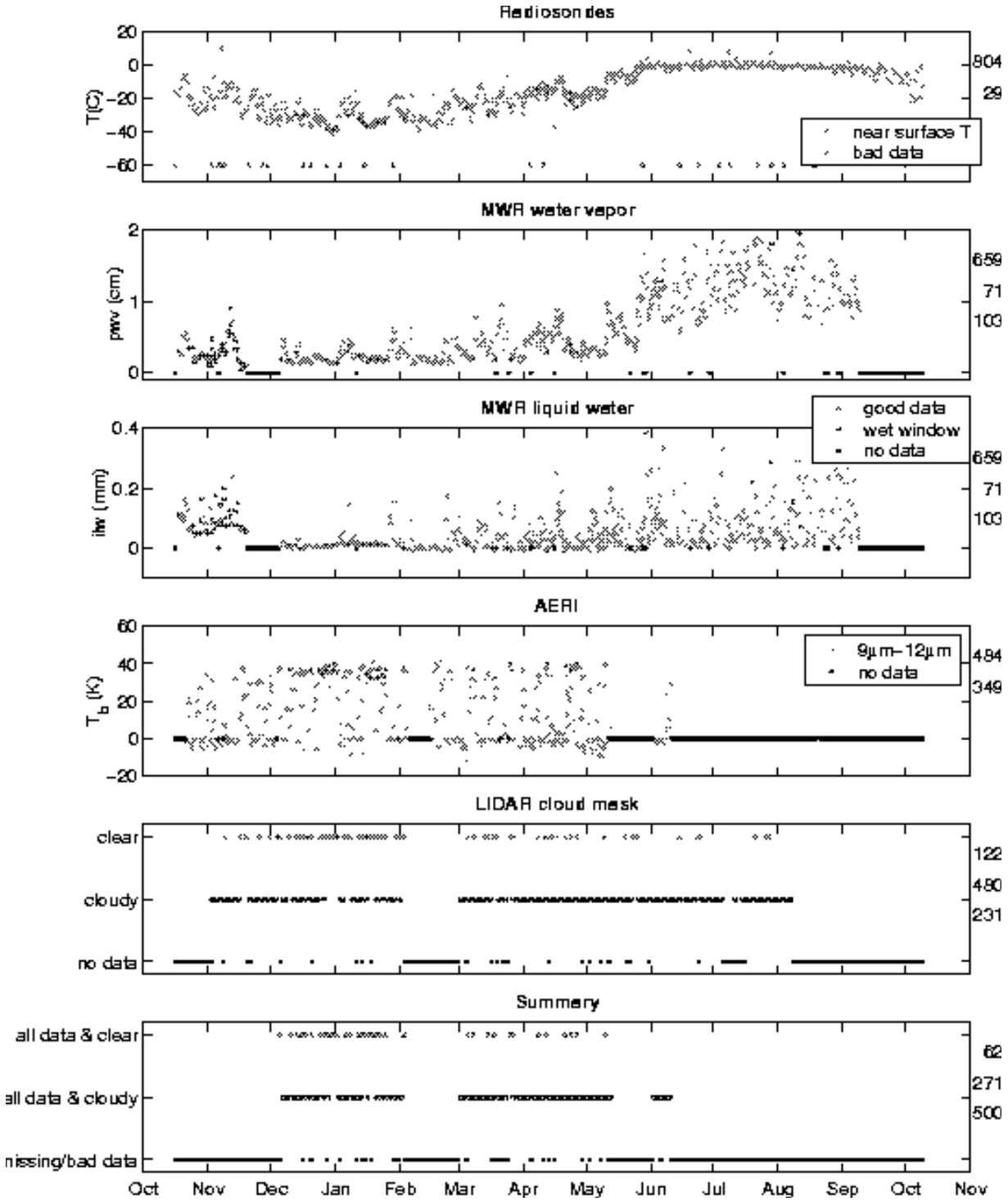


**Figure 2**. Time series of surface air temperature, integrated column water vapor, integrated column liquid water, AERI brightness temperatures differences, and cloud mask.

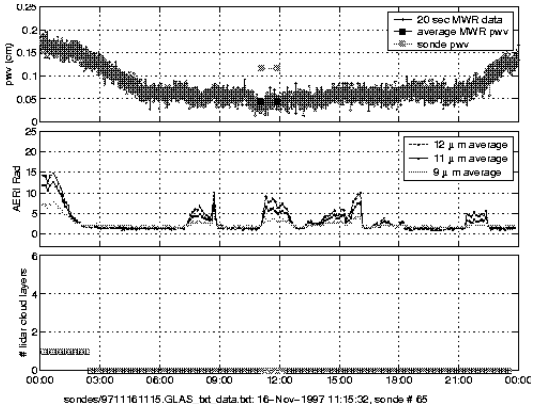


**Figure 3**. Example of an undetected cloud or AERI obstruction.

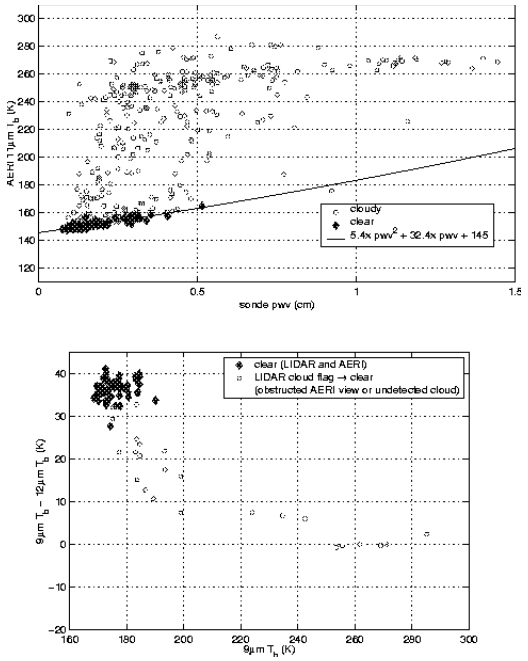


**Figure 4**. 11 μm AERI brightness temperatures.

5

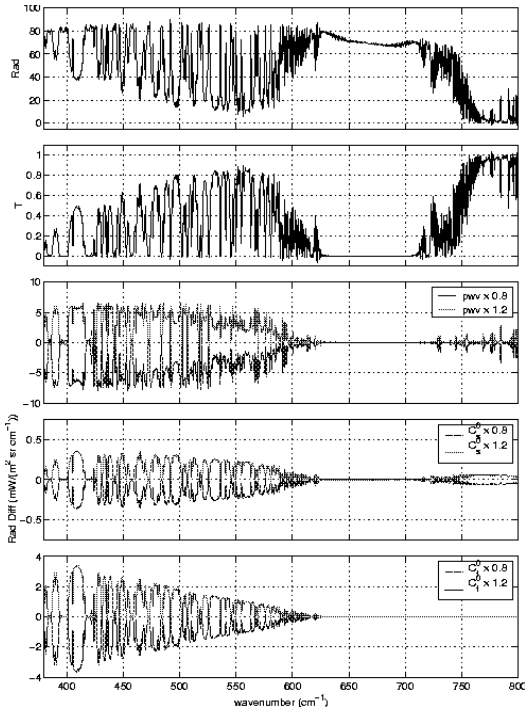


6

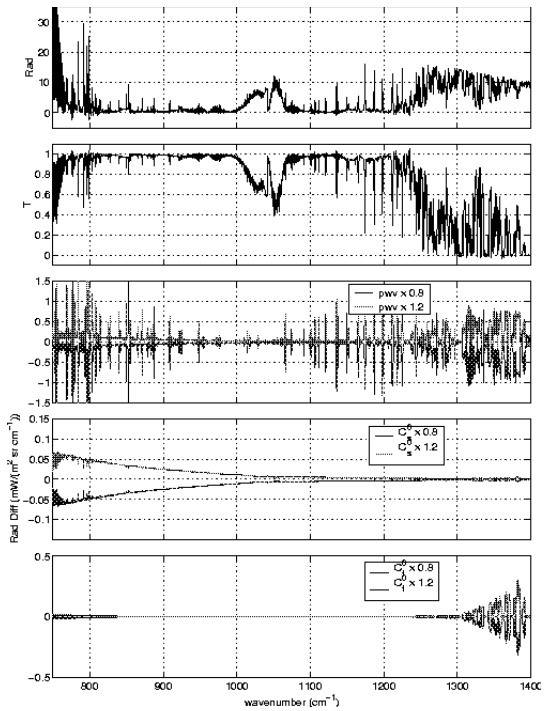


**Figures 5 and 6**. Downwelling radiance (top panel) and transmission (second panel) spectra computed with LBLRTM and the mean clear-sky radiosonde profile. Panels 3 through 5 show perturbations in the radiance calculations due to perturbations in the input water vapor profile and the self and air broadened water vapor continuum coefficients.

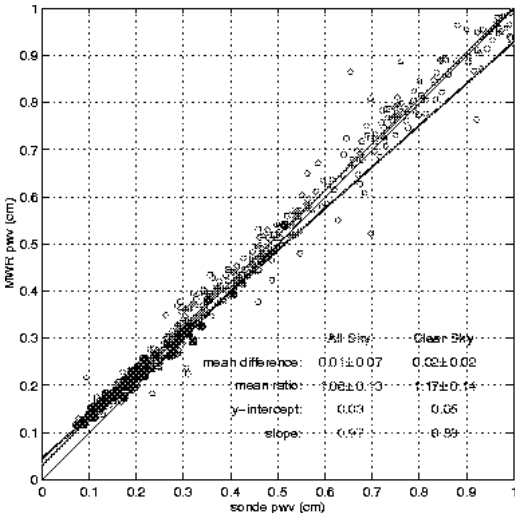


**Figures 7**. Scatter plot of radiosonde and CMWR pwv.

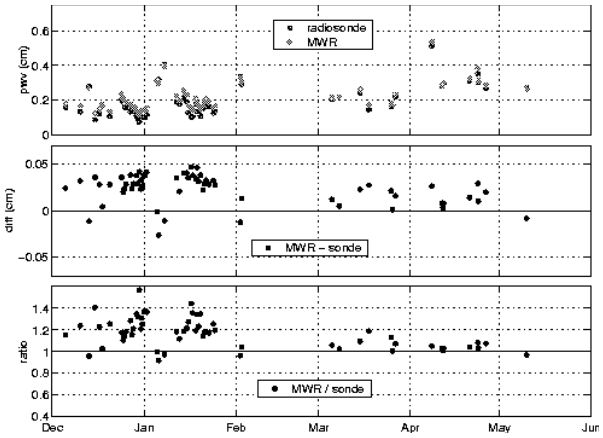


**Figure 8**. Time series of CMWR and sonde pwv.

## AERI Calibration Accuracy

The radiometric accuracy of the observed AERI radiances is primarily dependent on the knowledge and control of the on-board blackbody calibration sources. The contributions of the blackbody temperature and emissivity uncertainties to the uncertainty in the calibrated radiances for the SHEBA experiment are estimated in Figure 9, along with combined (RSS and absolute sum) uncertainties. Figure 10 shows a comparison of the NSA AERI-ER (identical to the SHEBA AERI-ER) to the prototype AERI before its

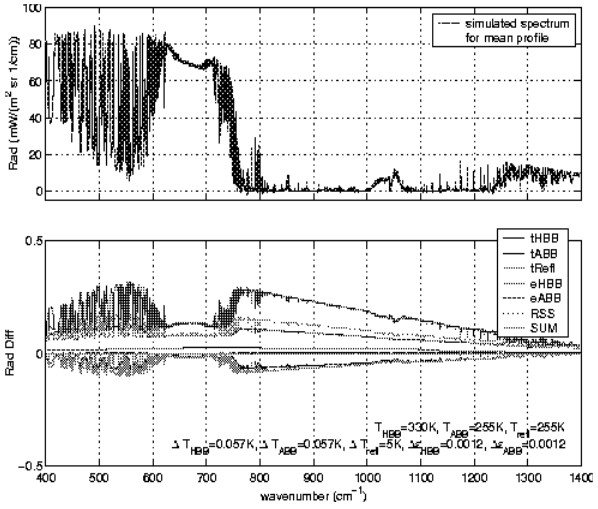


**Figure 9**. AERI calibration accuracy estimates systems based on calibration blackbody parameter uncertainties.

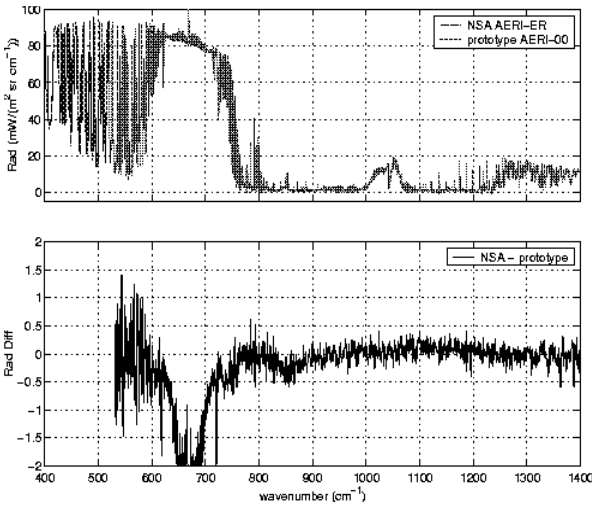


**Figure 10**. Differences between two AERI (NSA and prototype).

deployment to NSA, with window region differences less than ~0.25 rad units (The larger radiances differences between ~600 $cm^{-1}$ and 750 $cm^{-1}$ in this figure are due to temperature differences between the two instrument locations).

## Observed and Calculated Radiances

For each of the 62 clear-sky cases, downwelling calculations were performed and compared to the corresponding AERI observations. The calculations were performed using input water vapor profiles from the original radiosonde relative humidity profiles and with the sonde profiles scaled (independent of altitude) to have integrated column values equal to that of the CMWR.

The mean and standard deviation of the ensemble residuals are shown in Figure 11. The mean residuals throughout the 8-12 μm window are on the order of +1 rad units and show very little dependence on the input water vapor amount. Contamination by persistent aerosols, very large water vapor errors (i.e., +100% or +1mm), and/or unexplained AERI calibration errors are needed to explain these differences. The mean residuals for the 844 $cm^{-1}$ to 847 $cm^{-1}$ micro-window from these comparisons are plotted versus column water vapor in Figure 12 along with similar residuals from the analogous SGP site comparisons and various curves showing the effects of input water vapor and continuum perturbations and the AERI calibration accuracy. The residuals in the 400 $cm^{-1}$ to 600 $cm^{-1}$ region are more dependent on the input water vapor profile for these low water amounts, and the differences between the CMWR and radiosonde measurements are apparent in this spectral region. The mean residual due to the CMWR calculations are slightly negative (-2 rad units on average), whereas those due to the sonde pwv are slightly positive (+1 rad units on average). The standard deviation of the ensemble residuals for the CMWR scaled sonde calculations is roughly 2 times greater than those for the original sonde calculations. This is also evident in Figure 13, which shows the behavior of the 495 $cm^{-1}$ to 498 $cm^{-1}$ micro-window residuals. Using AERI as a stable reference and the calculations as a transfer, this suggests that the CMWR pwv measurements during SHEBA exhibit greater variability (with respect to AERI) than the sonde measurements. That is, the sonde-based calculations are better correlated with the AERI measurements than are the CMWR-based calculations. Recent findings suggest this is due to isolated situations (during SHEBA and certain time periods at NSA) where the CMWR is unstable due to thermal imbalance. Other features apparent in the mean spectral residuals are due to inaccurate ozone amounts, temperature profile errors, and water vapor spectral line parameters.

## Acknowledgements

We wish to thank Judy Curry, Wayne Feltz, Connor Flynn, Jim Liljegren, Dave Turner, Tony Clough, Taniel Uttal, Ed Westwater, and Yong Han for their help in this work.

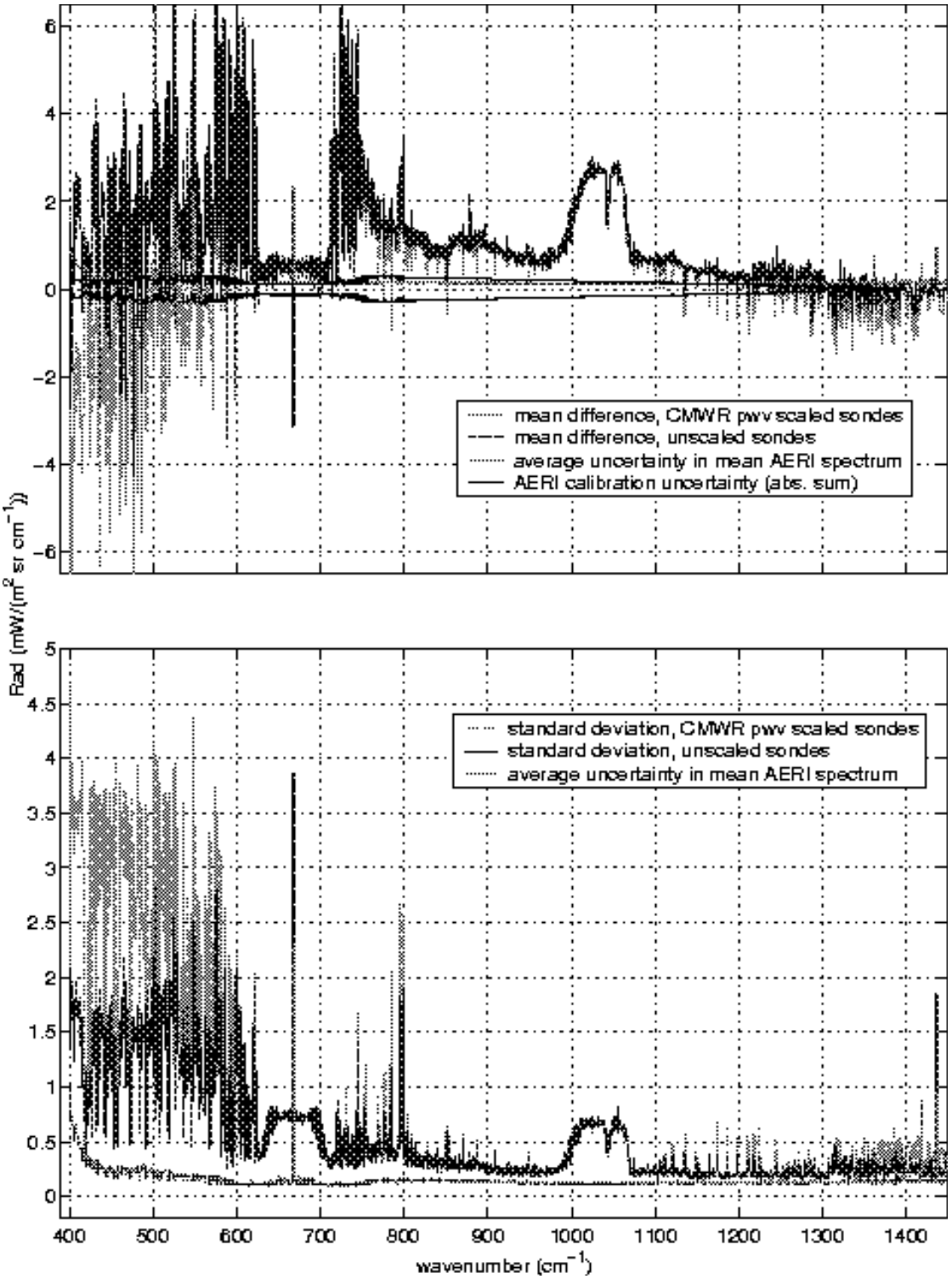


**Figure 11**. Mean and standard deviation of the ensemble residuals for the 62 clear-sky cases.

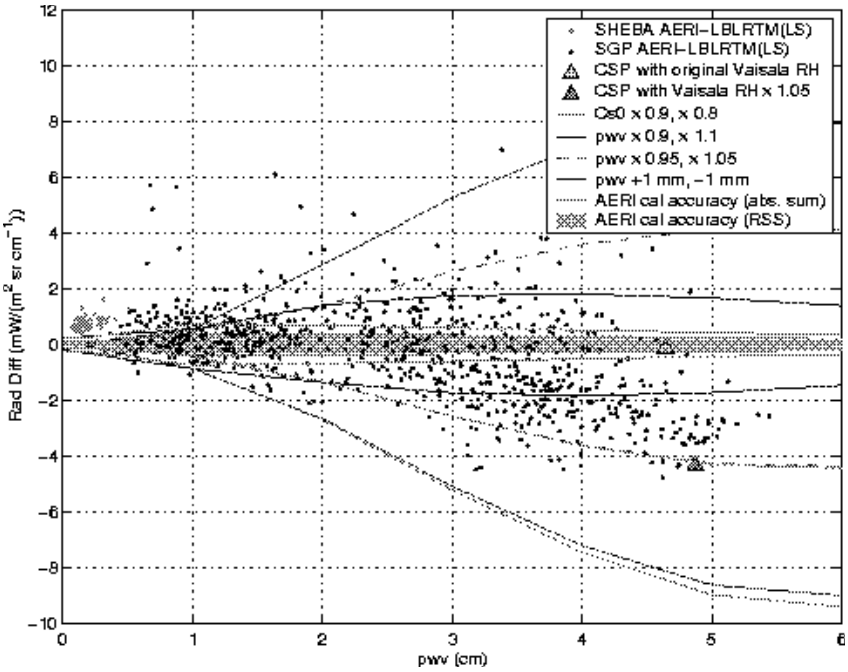


**Figure 12**. 844cm$^{-1}$ to 846 cm$^{-1}$ SHEBA and SGP residuals.

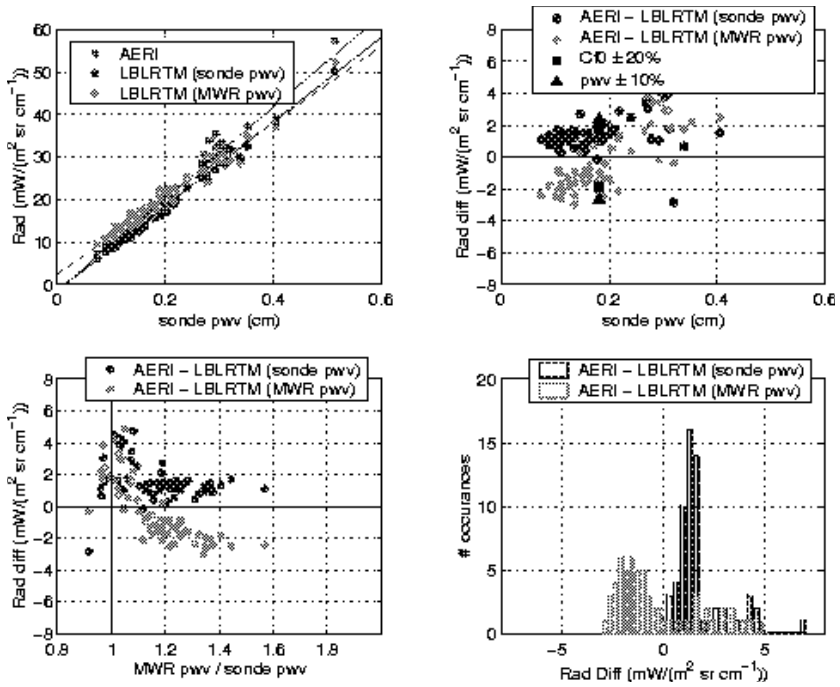


**Figure 13**. 495 cm$^{-1}$ to 498 cm$^{-1}$ SHEBA residuals.